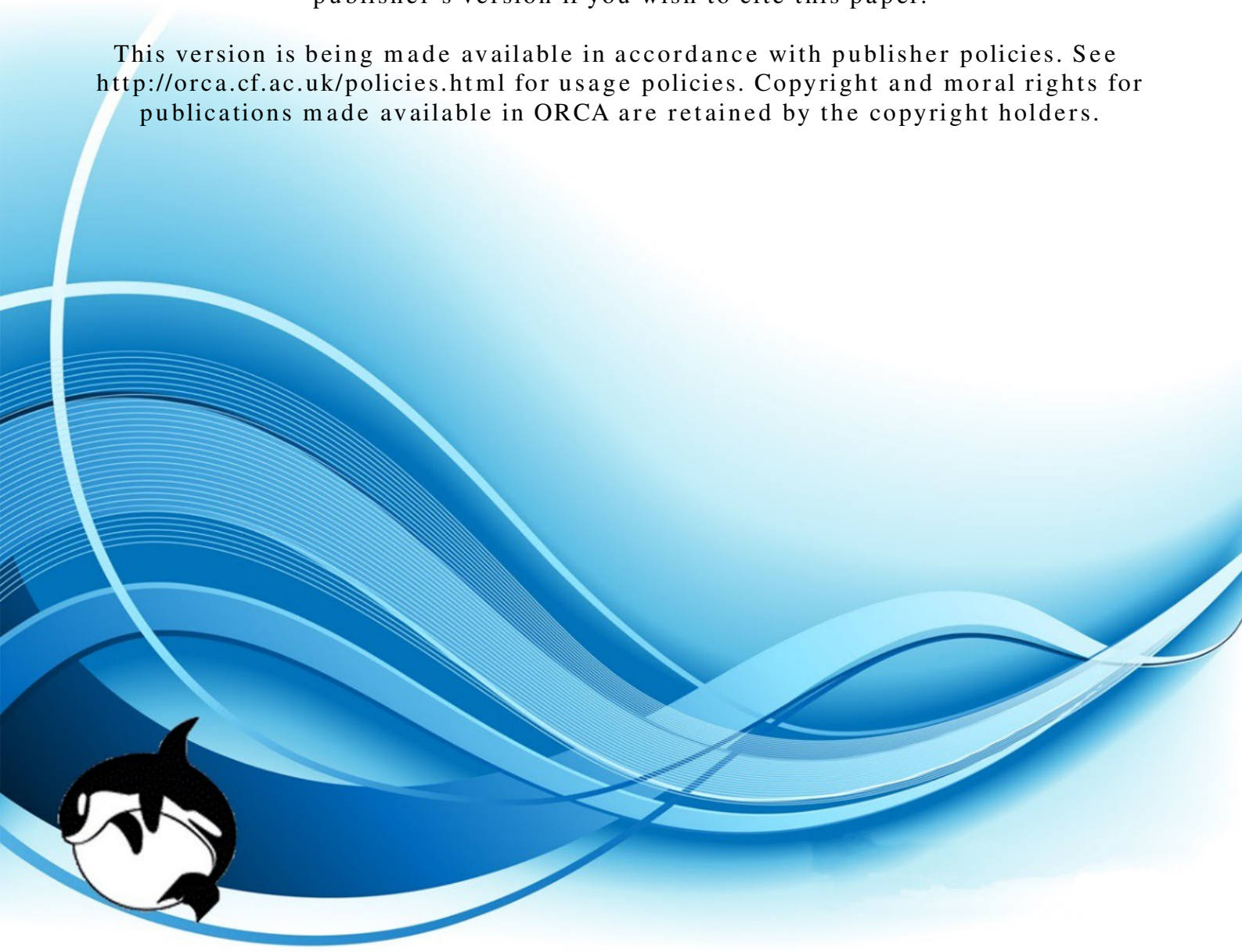

Evolution of disturbance wavepackets in an oscillatory Stokes layer

By **CHRISTIAN THOMAS**[1], **CHRISTOPHER DAVIES**[2], **ANDREW P. BASSOM**[3] AND **P. J. BLENNERHASSETT**[4]

[1]Department of Mathematics, South Kensington Campus, Imperial College London, London, SW7 2AZ, UK
[2]School of Mathematics, Cardiff University, Cardiff, CF24 4AG, UK
[3]School of Mathematics and Statistics, The University of Western Australia, Crawley, WA 6009, Australia
[4]School of Mathematics and Statistics, University of New South Wales, Sydney, NSW 2052, Australia.

(Received 3 June 2014)

Numerical simulation results are presented for the linear and nonlinear evolution of disturbances in a flat Stokes layer. The response to a spatially localised impulsive forcing is investigated and it is found that the spatial-temporal development of the flow displays an intriguing family tree-like structure, which involves the birth of successive generations of distinct wavepacket components. It is shown that some features of this unexpected structure can be predicted using the results of a linear stability analysis based on Floquet theory.

1. Introduction

We consider the Stokes layer that is generated by the motion of an infinitely long and flat rigid wall, oscillating sinusoidally to-and-fro within its own plane, beneath an unbounded body of viscous fluid that would otherwise remain stationary. The flow is described by one of the few known exact solutions to the Navier-Stokes equations. It can thus be construed as providing the archetypical boundary layer for the purpose of identifying the stability characteristics of unsteady flows.

Time-periodic flows involving a Stokes layer appear naturally in a wide variety of physical configurations, including coastal mechanics and physiological problems. For example, Womersley (1955) has shown that large frequency oscillatory blood flow in an artery can be described by invoking a Stokes layer immediately adjacent to the artery wall, along with an outer region of inviscid flow at locations further away. The existence of a range of potential applications has helped to motivate the considerable number of experimental and theoretical studies of the Stokes layer that have already been completed to date. The present paper provides a further theoretical contribution, by considering the spatial and temporal development of Stokes layer disturbances that are initially highly localized along the oscillating flow direction, after they have been triggered by an impulsive form of excitation. Previous stability studies have tended to focus on the temporal evolution of disturbances that are spatially monochromatic, with a single prescribed streamwise wavenumber. Our study is of a more general nature, since we shall consider disturbance wavepackets that are comprised of a continuous range of wavenumbers. Using results obtained from numerical simulations, it will be demonstrated that the behaviour of such

wavepackets in Stokes layers has a far more intricate and interesting structure than is commonly found for cases where the boundary layer is steady.

Extensive reviews of the stability of Stokes layers are available within the literature. An early account was given by Davis (1976), which contains details of the problem formulation and other relevant tools for investigating the stability of time-periodic boundary layers. It is only in relatively recent years that the Stokes layer has been shown, conclusively, to be unstable to linear disturbances. So we believe that it is helpful to include here a brief account of the history of investigations of the flow and some of the difficulties met in previous studies, which have aimed to piece together various stability results and experimental observations of the transition process.

The Stokes layer is characterised by a boundary layer thickness $\delta = \sqrt{2\nu/\omega}$, where ν is the kinematic viscosity of the fluid and ω the frequency of the oscillating wall. For a given velocity amplitude of the wall motion U_0 an appropriate Reynolds number $R = U_0/\sqrt{2\nu\omega}$ can be defined and used to designate regions of instability and the location of any transition to turbulence. As would be expected, physical experiments conducted on the Stokes layer reveal that the flow is unstable once R is sufficiently large. Although the standard Stokes layer consists of a semi-infinite region of fluid, layers that are bounded by a single planar wall are difficult to set up experimentally. As a result, most practical investigations are carried out either in a wide channel or within a cylindrical geometry. When the frequency of the imposed oscillations is taken to be sufficiently large, a flow that closely resembles a planar Stokes layer can be generated at the bounding wall surfaces. Stokes layers in cylindrical systems have been created by some experimentalists by allowing the pipe itself to oscillate back and forth, see for example Clamen & Minton (1977), whilst others have used a piston driver to force the fluid motion in a stationary pipe (Merkli & Thomann 1975; Hino, Sawamoto & Takasu 1976; Eckmann & Grotberg 1991; Akhavan, Kamm & Shapiro 1991a). Values of R ranging anywhere from 140 to 270 have been quoted as giving the location for when the Stokes layer first becomes unstable, with the particular critical value depending upon the particular experimental study concerned and the method used to generate a Stokes layer.

1.1. *Studies using Floquet theory*

A number of theoretical investigations of the planar Stokes layer have been carried out using various kinds of linear analysis, where governing equations for infinitesimal perturbations are derived. Owing to the time periodic nature of the flow, any mathematically rigorous and exact treatment of the stability problem should be based on Floquet theory, which seeks to directly determine the net growth or decay of a disturbance over a full cycle of the wall oscillation. In Floquet theory, modes of perturbation from the basic state are decomposed to contain the product of a time-periodic function $f(t)$ and an exponential function $\exp\{\mu t\}$, where the real part of the exponent μ determines the overall growth (or decay) and the periodic function $f(t)$ can be represented in the usual way using a Fourier series. This kind of approach to the stability problem was first formulated and applied to an instance of a finitely confined Stokes layer by von Kerczek & Davis (1974), while the semi-infinite layer case was tackled later by Hall (1978). In the finite Stokes layer calculation, an oscillating wall was placed at a distance 8δ beneath a stationary wall, but no instability was discovered for Reynolds numbers up to 400. For the infinite case, Hall (1978) found only decaying instabilities for Reynolds numbers below 160. Unfortunately, these early studies were all restricted to relatively small Reynolds number calculations.

With the advancement of computer resources Akhavan, Kamm & Shapiro (1991b) were able to extend the numerical investigation of the Stokes layer stability problem to

higher Reynolds numbers approaching $R \sim 500$. However, they still could not detect any evidence of unstable modes. It was not until a much later study was completed by Blennerhassett & Bassom (2002) that unstable Floquet modes were first found. The critical point for the onset of instability was determined to be located at about $R \sim 708$, with a corresponding wavenumber $a \sim 0.38$.

Thomas, Bassom, Blennerhassett & Davies (2010) conducted some direct numerical simulations of linearized disturbances developing in the Stokes layer, with the intent of confirming, or otherwise, the results of Blennerhassett & Bassom (2002) and obtaining information on the development of Floquet modes from an initial impulsive disturbance. The simulation results successfully matched the neutral stability curve found in Blennerhassett & Bassom (2002) and also indicated that the Floquet disturbance structure was established within three oscillation cycles of the basic flow.

1.2. *Some issues arising from physical experiments*

As has already been mentioned above, the Stokes layer configured in physical experiments has not been observed in an undisturbed form for Reynolds numbers much beyond about 270, which is little more than a third of the critical value for the onset of Floquet instability determined by Blennerhassett & Bassom (2002). One plausible explanation forwarded for this large apparent discrepancy is that it arises because the majority of experiments have been conducted in pipes rather than an unbounded planar geometry. In order to address this possibility, Blennerhassett & Bassom (2006, 2007) extended their investigations to include oscillatory flow confined within both cylindrical pipes and two-dimensional channels. Instability was again located and for wide enough channels or pipes results identical to those obtained for the unbounded planar configuration were recovered. At most, the confined geometry only caused a lowering of about 20% in the critical Reynolds number for a narrow range of pipe sizes, thus still leaving a large discrepancy between theoretical prediction and experimental observations. Wall roughness and external noise have also been proposed as providing possible explanations for why disturbances seem to be detected much earlier in practice than would be expected from the theory. Blondeaux & Vittori (1994), Verzicco & Vittori (1996) and Vittori & Verzicco (1998) have all modelled the effects of wall roughness on the Stokes layer and demonstrated that imperfections in the experimental apparatus can prompt the onset of a so-called quasi-steady mode of instability.

It should be mentioned here that we will not attempt to directly address any of the above issues associated with the configuration of physical experiments and the results that are obtained from them. However, it will be seen that our numerical simulations suggest that significant difficulties in the interpretation of experimental data are likely. These may arise both from the complex nature of the linearized impulse response that we have discovered, as well as from the rapid onset of nonlinearity that may be predicted unless noise levels are kept extremely low.

1.3. *Quasi-steady instability theories*

Quasi-steady instability theory is the term coined for all manner of approximate linear analyses, which are characterised by a simplification in which the profile of the basic state is frozen and treated as if it were steady, while the phase of the time within the oscillation cycle is relegated to the role of a parameter. A great attraction of quasi-steady theory is that it allows an Orr-Sommerfeld equation to be considered, which leads to a prediction of an instantaneous growth rate for each instant within a cycle of the underlying flow. Over some parts of the cycle, the frozen profiles are found to become highly unstable at Reynolds numbers well below the critical value of 708 given by Floquet

theory. The drawback of the quasi-steady approximation is that it can only be strictly justified in the limit $R \to \infty$. Both Cowley (1987) and Hall (2003) have conducted quasi-steady calculations for large R but the unstable modes found turned out not to have any periodic dependency with respect to the oscillation phase of the basic state.

A more recent investigation by Luo & Wu (2010) has provided further insight into the relationship between the results obtained using a quasi-steady analysis and those from Floquet theory. For a given wavenumber, numerical simulations were conducted to solve the initial value problem for disturbances evolving in an oscillating channel with a large half width. The behaviour of the numerical solutions was found to be in excellent accord with the instability results obtained from Floquet theory by Blennerhassett & Bassom (2002). Furthermore, it was shown that the eigenfunction structure in the Floquet solution is well approximated by the quasi-steady eigenfunctions, at least over significant parts of the basic flow cycle.

1.4. *Impulse response and the present study*

The current investigation examines the spatial and temporal development of impulsively excited disturbances, that are initially localised in space within a Stokes layer. The motives for considering wavepackets, rather than purely monochromatic waves, are similar to those which have driven studies of absolute and convective instabilities in steady flows. (See, for example, the account included in the book chapter by Huerre & Rossi (1998).) In general, the consideration of disturbances that are fully characterised by a single wavenumber does not suffice to determine the possibilities for disturbance development. Even when it is known that perturbations with chosen wavenumbers are unstable, this may not be enough to give rise to sustained temporal growth at any fixed point in space for physically realisable forms of disturbance. Observable disturbances will typically take the form of a wavepacket, comprised of a range of different wavenumbers, unless some artificial means can be found to preclude this. In many unstable flows, wavepackets always propagate away from any given spatial location, eventually leading to a quietened flow there, though the maximum disturbance amplitude still grows as it travels. Disturbances only display sustained temporal growth at a fixed point in space if it is possible to meet additional mathematical requirements that ensure that the instability has an absolute character.

Brevdo & Bridges (1997) extended the analysis of disturbance wavepacket development in steady boundary layers and shear flows to include cases of temporally oscillating flows. They found that it was possible to modify the techniques appropriate to a steady base flow so as to account for disturbance structures that are described by Floquet theory. In particular, they argued that the long-term behaviour of unstable wavepackets in unsteady flows could still be categorised using a twofold classification of instabilities as being either convective or absolute in nature.

When we come to consider our numerical simulation results it will be seen that, in a manner similar to the steady case, the growth of wavepacket maxima is dictated by the largest growth rate that can occur for a single wavenumber disturbance. This growth rate now needs to be computed by considering the growth exponents for Floquet modes, rather than those associated with the more simply structured normal modes that are relevant for a steady flow. Such a connection between Floquet theory and the growth of maximum amplitudes does not seem to have been formulated explicitly by Brevdo & Bridges (1997), but it would appear to be implicit in their work. We shall show that tracing growth using relationships of this general kind can be helpful in making sense of the behaviour of wavepacket disturbances in the Stokes layer. However, it will also be seen that the nature of the actual spatial and temporal development is much richer and

more interesting than might have been surmised by merely considering the asymptotic growth for large times.

In addition to simulating the linearized development of wavepackets, we will more briefly consider the fate of these disturbances when they become nonlinear. Mainly for reasons of computational economy, this will be in a somewhat artificially constrained setting, in which three-dimensional evolution is excluded. Such a restriction to two dimensions can be strictly justified for sufficiently small amplitude disturbances, by appealing to Squire's theorem, which still applies for oscillatory flows. However, it is likely that for larger amplitudes, important physical processes may be omitted. We shall show that there is still some interest in studying the onset of nonlinearity in such circumstances. For example, it will be seen that wavepackets with a relatively small initial amplitude can quickly grow and become subject to important nonlinear effects within a single oscillation period of the Stokes layer.

1.5. *Organisation of the paper*

Our aim is to study, via direct numerical simulation, the spatial and temporal evolution of disturbances that are locally generated by an impulsive forcing in a Stokes layer. The results for the structure of the developing wavepackets are rather novel and so our focus here is on a careful exposition of their characteristic form. Evidence is given to demonstrate that the unexpected nature of the behaviour that we have discovered is not due to any numerical artifices of our simulation method. Thus, we will begin in §2 with an account of the mathematical formulation and an outline of the numerical discretization scheme, which includes a brief description of the velocity-vorticity based methods that were originally developed by Davies & Carpenter (2001). The results for the linear evolution of the disturbance are discussed in §3, which is further divided into subsections, each focusing on a specific aspect of the flow behaviour. The most striking new feature of the simulation results is presented in §3.1, namely the family tree-like structure that is generated with distinct wavepacket components. Section 3.4 briefly describes how this structure is entirely compatible with it being formed from a linear superposition of spatially monochromatic waves, as would be considered in a Fourier decomposition. The growth properties of the wavepacket components are discussed from several points of view in sub-sections §§3.7–3.9, while the effect of the timing, with respect to base flow, of the initial impulse is shown in §3.10. After gaining some understanding of the linear behaviour for small amplitude disturbances, we move on to consider the nonlinear evolution. There is a focus on an initial phase of development during which, in the absence of nonlinear effects, the growth displayed by the disturbance could have taken a more transient form. The additional numerical constraints imposed by the nonlinear calculations are discussed first in §4.1 and §4.2, with the results obtained presented in the remaining sub-sections of §4. The paper closes with a few final remarks.

2. Mathematical formulation and numerical methods

We consider the two-dimensional flow of a semi-infinite body of viscous incompressible fluid that is bounded by a flat wall located at $y = 0$. The wall moves back-and-forth in the x-direction with a velocity $U_0\cos(\omega t)$, where ω is the oscillation frequency. This forces the adjacent body of fluid into a sinusoidal cycle of motion, giving a Stokes boundary layer with a thickness of $\delta = \sqrt{2\nu/\omega}$, where ν is the kinematic viscosity of the fluid. If lengths are scaled using δ, the velocities with the amplitude U_0 and the time is set as

$\tau = \omega t$, then the base flow for the Stokes layer is given by

$$U = U_B(y,\tau) = \mathrm{e}^{-y}\cos(\tau - y), \qquad V = 0. \tag{2.1}$$

2.1. *Governing equations for disturbances*

The development of disturbances from the basic flow (2.1) will be studied using a numerical simulation method that is based upon a two-dimensional version of the velocity-vorticity formulation that was first described by Davies & Carpenter (2001). The total velocity and vorticity fields are decomposed as

$$(U,V) = (U_B,0) + (u,v) \qquad \text{and} \qquad \Omega = \Omega_B + \zeta, \tag{2.2}$$

where $\Omega_B = U_B'$ is the undisturbed spanwise vorticity field that is associated with the base flow U_B. The streamwise and normal velocity perturbations are denoted by u and v, respectively, whilst ζ represents the vorticity perturbation.

The system of governing equations for the disturbances is given by the vorticity transport equation, coupled to a Poisson equation for the wall-normal velocity and an integral that defines the streamwise velocity. It takes the form

$$\frac{1}{R}\frac{\partial \zeta}{\partial \tau} + U_B\frac{\partial \zeta}{\partial x} + U_B''v + \underbrace{\frac{\partial (u\zeta)}{\partial x} + \frac{\partial (v\zeta)}{\partial y}}_{\text{nonlinear terms}} = \frac{1}{2R}\left(\frac{\partial^2}{\partial x^2} + \frac{\partial^2}{\partial y^2}\right)\zeta, \tag{2.3a}$$

$$\left(\frac{\partial^2}{\partial x^2} + \frac{\partial^2}{\partial y^2}\right)v = -\frac{\partial \zeta}{\partial x}, \tag{2.3b}$$

$$u = -\int_y^\infty \left(\zeta + \frac{\partial v}{\partial x}\right)dy, \tag{2.3c}$$

where the Reynolds number is defined to be $R = U_0\delta/2\nu \equiv U_0/\sqrt{2\nu\omega}$. The underbrace beneath the left hand side of the vorticity equation (2.3a) is deployed to highlight the two nonlinear terms that involve products of the perturbation velocity and vorticity fields. For the linearized simulations that will provide a major focus of this paper, these nonlinear terms are simply removed from consideration. The explicit expression (2.3c) for u has been obtained by recasting, in an integral form, the relation that defines the vorticity ζ, under the assumption that u approaches zero at large distances from the wall.

2.2. *Boundary conditions and excitation of disturbances*

Impulsive forcing, by means of a small localised vertical displacement $\eta(x,\tau)$ of the wall surface, is introduced for a very short period after $\tau = 0$, in order to stimulate the development of disturbances. When linearized about the undisplaced wall location, the no-slip and no-penetration conditions take the forms

$$u = -U_B'(0,\tau)\eta, \tag{2.4a}$$

$$v = \frac{\partial \eta}{\partial \tau}, \tag{2.4b}$$

both of which are applied for $y = 0$. We chose to set

$$\eta = A\,\mathrm{e}^{-\lambda_f (x-x_f)^2}(1 - \mathrm{e}^{-\sigma\tau^2})\mathrm{e}^{-\sigma\tau^2}, \tag{2.5}$$

where A is a non-zero constant, λ_f is a scaling factor that was selected so as to determine a very narrow streamwise extent for the forcing, x_f is the streamwise location of the centre of the impulse and the parameter σ characterises its duration. The value of A was

used to provide a measure of the initial disturbance size when the effects of nonlinearity were being investigated, but of course could be chosen arbitrarily for studies of the linearized disturbance development. It is evident that the forcing is only significant during a time interval $\tau \sim 1/\sqrt{\sigma}$, which can be made suitably small by taking σ to be large. We chose to allow the impulse to endure for less than one twentieth of an oscillation cycle, which ensured that a wide range of possible response frequencies for the disturbance were seeded into the flow. After this initial forcing period $\eta \to 0$, so that the configuration of an undistorted wall, where u and v both vanish, is recovered. The linearized conditions (2.4*a*), (2.4*b*) were also retained when simulating the nonlinear development. This was possible because the disturbances were always triggered by a very small amplitude impulsive wall distortion.

The no-slip condition, which needs to be applied when determining the vorticity perturbation ζ using the transport equation (2.3*a*), can be rewritten in the form of an integral constraint. This is derived by substituting (2.4*a*) into the definition (2.3*c*) and then rearranging to give

$$\int_0^\infty \zeta dy = U_B'(0,\tau)\eta - \int_0^\infty \frac{\partial v}{\partial x} dy, \tag{2.6}$$

which is fully equivalent to the no-slip condition on u. Equation (2.4*b*) provides the boundary condition at the wall for the normal velocity perturbation v that is needed in order to solve the Poisson equation (2.3*b*). Suitable boundary conditions on the disturbance far away from the wall are obtained by simply requiring that the perturbations ζ and v both tend to zero for $y \to \infty$.

2.3. *Numerical methods*

The numerical methods adopted for the discretization of the governing equations (2.3) are discussed in detail in Davies & Carpenter (2001) and were reviewed by Thomas, Bassom, Blennerhassett & Davies (2010), so only a brief overview of the scheme is given here. Streamwise derivatives are approximated using a fourth-order centred, compact finite difference scheme. Along the wall-normal direction, the perturbations ζ and v are expanded in terms of odd Chebyshev polynomials for a mapped wall-normal co-ordinate $\xi = L/(L+y)$, where L is a stretching factor that fixes the resolution distribution across the width of the Stokes layer. The change of variable maps the semi-infinite physical domain $y \in [0, \infty)$ onto the computational domain $\xi \in (0, 1]$. A similar series expansion is applied for u, but now making use of only even Chebyshev polynomials of ξ. Each of the governing equations (2.3*a*) and (2.3*b*) is integrated twice with respect to ξ, in order to obtain a simple banded structure for the matrices that discretize the operators applied to the wall-normal variation. This allows spectral accuracy to be obtained in the wall-normal direction, without incurring any significant increase in the computational expense above that needed for a finite-difference scheme. The time marching is treated using a semi-implicit procedure.

Successful simulation of the disturbance development was achieved after careful choices were made for the following parameters in the numerical discretization: (i) the time step $\Delta\tau$; (ii) the streamwise increment Δx; (iii) the number N of distinct Chebyshev polynomials deployed for the series expansions along the wall-normal direction and (iv) the mapping parameter L. For the linearized simulations, well resolved and numerically stable results could be obtained using a time step $\Delta\tau \sim 0.1/R$ and a streamwise grid with $\Delta x \sim 1$. The resolution requirements for studying nonlinear disturbances were found to be more demanding, since it was then necessary to capture the evolution of the much smaller scale features that could then arise. A spatial increment $\Delta x \sim 0.05$ was needed,

which required a corresponding decrease in the time step to $\Delta\tau \sim 0.01/R$ to ensure that numerical stability was retained. Setting the mapping parameter to be $L = 5$ was found to give a suitable spread of points along the wall-normal direction. Upwards of $N = 100$ Chebyshev polynomials were needed in order to encapsulate the wall-normal variation of the disturbances. Taking N to be much smaller than this caused a very quick and unphysical breakdown in the simulation results.

We conducted numerical tests that gave us confidence that only marginal changes would be expected from further increases in the resolution, beyond those that we eventually settled upon. Tracing such minor changes would not have justified the additional computational resources and run-time requirements that would have then become necessary.

2.4. *Computational domain and the inflow/outflow boundaries*

Another significant non-physical variable that needed to be settled was the streamwise extent X of the computational domain. Typically, the impulse that excited the disturbance was applied at a position towards the middle of the domain. It was necessary to ensure that, as time passed and the disturbance spread away from its initial central location, there were no artificial reflections arising at the streamwise boundaries, or any other unphysical perturbations triggered by their presence. If X was taken to be too small, numerical noise could appear at the outer boundaries and slowly grow in magnitude, propagating towards the genuine part of the computed disturbance. It proved necessary to always take the extent of the domain to be sufficiently large so as to be sure that no physically significant disturbance could approach the computational boundaries, throughout the whole of the time interval for which the simulation was being conducted.

At one boundary of the computational domain, null perturbation conditions $v = \zeta = 0$ were imposed; at the other boundary wavelike outflow conditions were implemented Kloker *et al.* (1993). Both of these conditions were originally developed for other flow configurations containing a steady flow component where disturbances were required to convect out of the computational domain without the onset of any spurious reflection effects. Here there is no mean flow and the main reason that we persisted in applying different boundary conditions at the two ends of the domain was that this combination of conditions was already known to be very robust (see, for example, the appendix of Davies & Carpenter (2003)). As a check on the viability of the conditions applied at the computational boundaries, simulations were conducted with the direction of the Stokes flow reversed by the application of a half-period time shift, but without any interchange of conditions at the spatial extremities of the computational domain. The simulation results that were then obtained perfectly reproduced the expected reflection symmetry for the perturbation flow fields, thus confirming that no spurious effects were being introduced by the asymmetric treatment of the two boundaries of the computational domain. Some further details are given later.

Before deciding upon the above treatment of the inflow and outflow boundaries, buffer regions were also introduced and tested in an attempt to discover whether it might be feasible to make use of smaller computational domains. However, it was found that, at least for the particular buffer methods that were implemented, this only served to accelerate the onset of numerical noise and its spurious superposition with the genuine disturbance. As a consequence, very large streamwise domains were required, with a typical length $X \sim 6000$ or greater being deployed for the linearized simulations. It should be noted that the most unstable forms of disturbance were associated with waves that had a characteristic length scale $\lambda \sim 15$, which meant that for $X \sim 6000$ the computational domain was spread over $X/\lambda \sim 400$ wavelengths. A reduction to $X \sim 2000$ was made for

the simulation of nonlinear disturbances, in order to accommodate the necessary increase in grid resolution, without placing excessive demands upon the available computational resources. This meant that the simulation time intervals that could be considered for the nonlinear disturbance evolution had to be curtailed accordingly, so that disturbances did not have enough time to reach the artificially imposed boundaries.

3. Linearized simulation results

As has already been mentioned, a major concern of the present paper is the investigation of the evolution of linearized disturbances. We will describe the response to a spatially localised impulse, for various values of the Reynolds number which were chosen to be in the vicinity of the critical value for the onset of Floquet instability.

3.1. *Family tree spatial-temporal structure*

The first case that we consider is for a disturbance excited at a Reynolds number $R = 600$ so that, according to the linear Floquet analysis of Blennerhassett & Bassom (2002), it should be expected to decay. The impulse is applied at the streamwise location $x_f = 3000$, the centre of the chosen computational domain $0 \leqslant x \leqslant 6000$, thus maximising the distance that propagating disturbances would have to travel in either direction before reaching the location of any artificial outer boundary. The phase in the oscillation cycle at which the disturbance was excited is given by taking $\tau = 0$ in the expression (2.1) that defines the basic state. This coincides with the wall velocity achieving its maximum magnitude and being oriented along the direction in which x increases.

The resulting spatial-temporal development of the disturbance wavepacket is plotted in figure 1a, for three cycles of the wall oscillation and over the interior range of streamwise locations $1500 \leqslant x \leqslant 5500$. The amplitude $|\zeta|$ of the disturbance has been measured using magnitudes obtained from envelopes that were constructed to encompass the oscillatory spatial variation of the perturbation vorticity along the bounding wall surface. For each instant of time, an envelope was computed by applying a Hilbert transformation to the wall vorticity simulation data. (An example snapshot of the x-dependent wavepacket behaviour, together with the corresponding envelope, is presented later in figure 3.) The amplitudes are displayed using a shading that is defined with a logarithmic scaling. A finite, though relatively very small, cut-off level for the magnitude has also been deployed, so as to provide a threshold for detecting the presence or apparent absence of a perturbation at any given spatial-temporal point. The use of this threshold gives rise to the white background that is seen in the plot, which helps to clearly delineate the boundaries of the regions where the disturbance has developed. Subsequent figures display plots that were similarly constructed. (In the grey-shaded versions of these plots, the indicated gradation means that some whitened features can be found which are completely enclosed within regions where the disturbance has an appreciable magnitude. However, it may easily be discerned that such white colouration no longer indicates a perturbation amplitude that lies below the cut-off.) It should be noted that the use of a logarithmic scaling serves to ensure that the qualitative features of the disturbance development that we shall identify are relatively independent of the measure of the disturbance amplitude that has been chosen. The use of amplitudes based on physically relevant quantities other than the perturbation wall vorticity would, of course, be expected to lead to alterations in some of the finer quantitative details. Nevertheless, it can be anticipated that these will not be enough to give rise to any order of magnitude changes that could have a marked effect on logarithmic values, such as would be required to produce significant shifts in the locations that are picked out for individual wavepacket components of the disturbance.

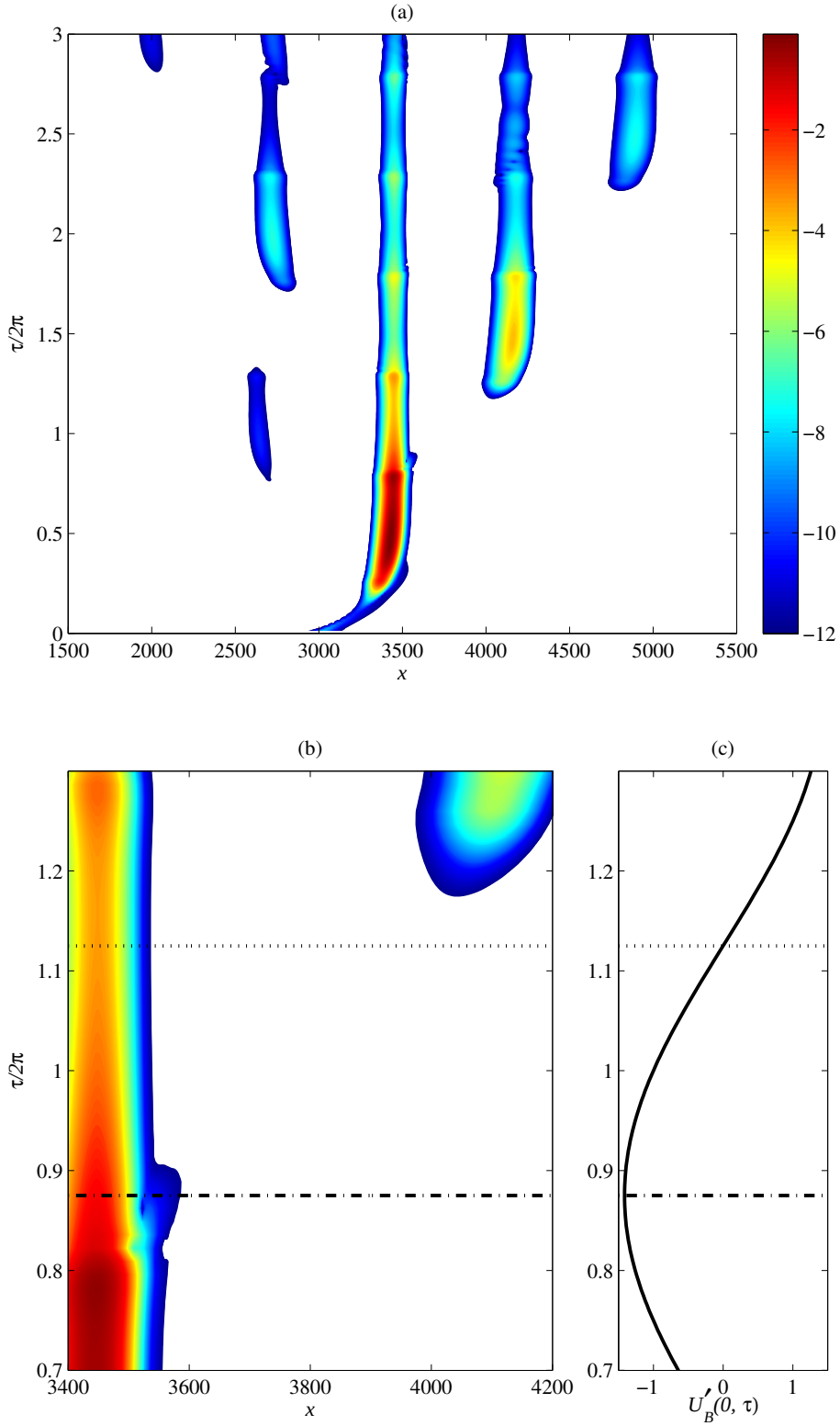

FIGURE 1. (a) Spatial-temporal development of the vorticity magnitude $|\zeta|$ at the wall surface, for a disturbance that was impulsively excited at $x_f = 3000$ for $R = 600$. (The magnitudes are plotted using a natural logarithmic scale for the shading); (b) Localized development about the first 'birthing' position; (c) Time variation of the wall shear stress $U_B'(0, \tau)$ for the basic flow.

It may be seen from figure 1a that, initially, the perturbation propagates to the right of the impulse origin $x_f = 3000$, which is downstream with respect to the basic flow near to the wall at the time that the disturbance was excited. The disturbance grows in magnitude until it attains a maximum amplitude near to the streamwise position $x = 3500$ at around the time $\tau = \pi$. At approximately the same time and position in the spatial-temporal plane, a secondary or *daughter* perturbation is created from the original *mother* wavepacket, propagating to the left. It may be noted that this new propagation direction matches that of the wall motion for the corresponding part of the oscillation cycle. The *daughter* wavepacket is of smaller amplitude than its *mother* and attains a maximum magnitude at the end of the first period before it diminishes. A second *daughter* wavepacket is born from the *mother* at the end of the first cycle. This now propagates to the right, growing to a larger amplitude than the first *daughter* and attaining a maximum magnitude at about the time $\tau = 3\pi$ in the vicinity of $x = 4200$. The original *mother* wavepacket continues to give birth to new *daughter* wavepackets, which alternate between propagating to the left and to the right. In turn, the *daughter* wavepackets give birth to *grand-daughter* wavepackets, which also display a switching in propagation direction, dependent upon the orientation of the wall motion during the half period in which they arose. The process of wavepacket birthing continues indefinitely and a disturbance with a *family-tree* like structure is formed.

3.2. *Birth timings for wavepacket components*

Figure 1b depicts the spatial-temporal development of the same disturbance as before, but now the plot has been centred and magnified around the location where the mother wavepacket gives birth to a daughter, which moves to the right. The shaded region that encompasses the mother disturbance displays a bud-shaped protuberance at about the time $\tau = 7\pi/4$ (marked by the chain line), which seems to lead to a daughter wavepacket that only becomes visible again after the time $\tau = 9\pi/4$ (dotted line). As can be seen by making reference to figure 1c, the first of these two particular time instants coincides with when the gradient of the basic flow at the wall $U'_B(0,\tau)$, which defines the wall shear stress, takes a minimum value. The second is associated with the reversing of the shear stress from negative to positive values. The birthing events for other daughter and grand-daughter wavepackets are also found to be positioned at times where $U'_B(0,\tau)$ is a minimum (for those wavepackets that move to the right; at times $\tau = 7\pi/4 + 2\pi k$, where $k = 1, 2, 3, \ldots$) or a maximum (for wavepackets propagating to the left; $\tau = 3\pi/4 + 2\pi k$). Following an apparent period of decay, at least with respect to the amplitude measured using the perturbation vorticity at the wall, the offspring wavepackets can only be clearly distinguished again once they have started to grow, during the times just after $U'_B(0,\tau)$ has vanished ($\tau = \pi/4 + \pi k$). It had previously been noted by Cowley (1987), in his investigation of the Stokes layer using a quasi-steady approximation at the inviscid limit, that the most rapid increase in the perturbation amplitude occurs in the time interval that follows the reversal in the sign of the wall shear stress. This result appears to be consistent with our findings for the impulsively excited disturbance development. The results found in the simulations would also seem to agree with the experimental study of Clarion & Pelissier (1975), where it was observed that disturbances appeared in the Stokes layer soon after phases in the oscillation cycle when there was flow reversal adjacent to the wall.

3.3. *Transient growth from superpositions*

Eventually, two or more individual wavepackets components can propagate into the same region of space and overlap each other. At these locations, the superposition can cause

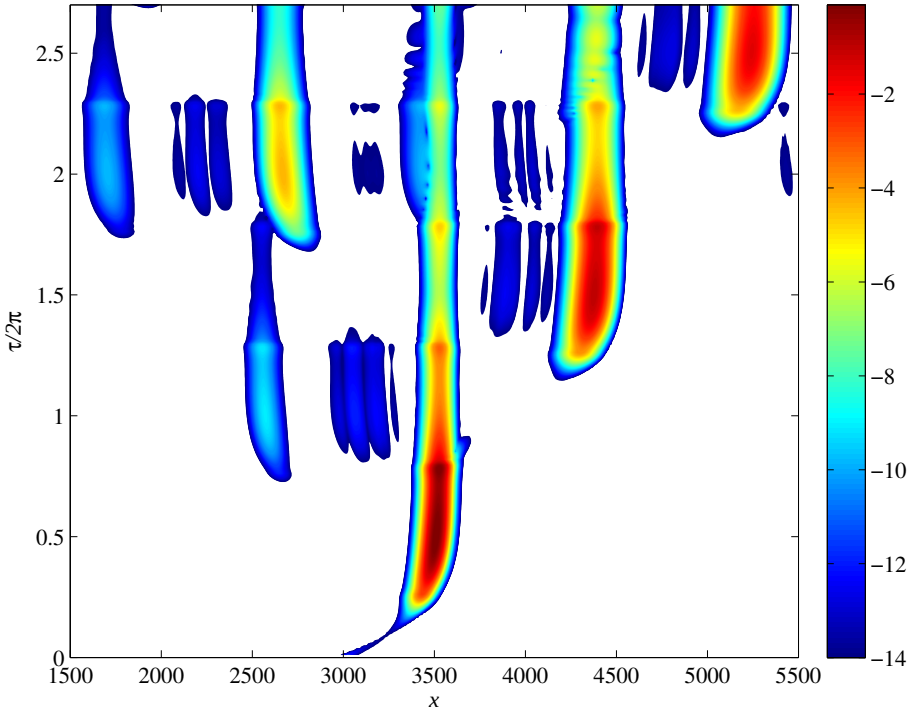

FIGURE 2. Spatial-temporal development of $|\zeta|$ at the wall surface, for a disturbance impulsively excited at $x_f = 3000$ for $R = 700$. (The shading that is used to display the amplitudes again deploys a natural logarithmic scaling. In both this figure and the previous one for $R = 600$, the amplitudes have been normalised so as to have ~ 1 maximum values. The larger disturbance growth exhibited for $R = 700$ is reflected in an increased range of plotted logarithmic values.)

there to be a relatively short interval of transient temporal growth. Figure 2 provides a clearer illustration of the kind of overlapping that can occur between different wavepacket components, each of which was originally distinct. The plotted structures depict the disturbance development that was obtained from a simulation conducted with a Reynolds number $R = 700$. This increased value of R yields disturbances that are relatively long lived, since it is only marginally lower than the value associated with the onset of linear instability (Blennerhassett & Bassom 2002). Although an overall decay is still observed for asymptotically large times, there is more time for initially separate components to interact and produce transient local growth. A careful examination of the depicted disturbance development reveals that, near to the streamwise location $x = 3500$ and over a range of times around $\tau = 4\pi$, the original mother wavepacket and a secondary or grand-daughter wavepacket have become overlapped. Such behaviour is not restricted to just this one occurrence. For example, a close inspection of the space-time region in the neighbourhood of the point $(x, \tau) = (4200, 4.6\pi)$ also indicates that there has been a wavepacket superposition. Indeed, both for this particular numerical simulation and for others that were conducted, overlaps could be traced for many of the individual wavepackets components. These tended to occur more and more commonly as the family-tree structure developed over time, as well as becoming more pronounced when the Reynolds number was increased.

Figure 3 shows the spatial variation of the wall vorticity, at a particular time instant

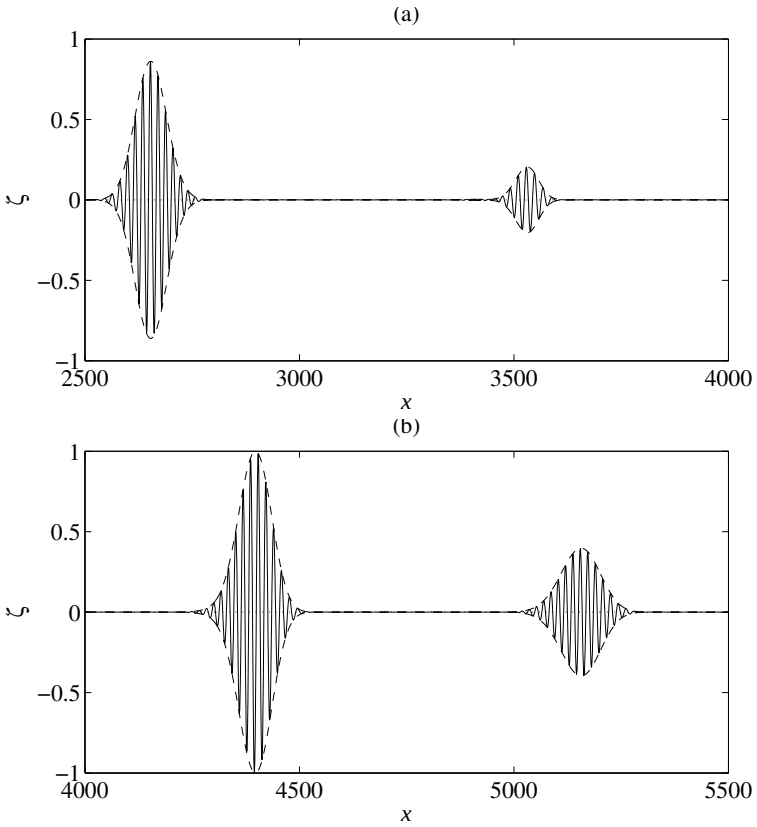

FIGURE 3. Perturbation wall vorticity ζ at the time $\tau = 4.5\pi$, for a disturbance impulsively excited at $x_f = 3000$ for $R = 700$. (This corresponds to taking a line at $\tau/2\pi = 2.25$ through the structure that was shown in figure 2.) The spatial variation displayed in (a) is continued in (b). The dashed lines plot the envelopes $\pm|\zeta|$ constructed using a Hilbert transform.

$\tau = 4.5\pi$, for the same simulation as was considered in figure 2. It thus illustrates, in greater detail, the x-dependent behaviour that is found along a chosen horizontal slice through the previously depicted family-tree structure. Four distinct wavepacket components can be clearly discerned. These may be identified as the mother wavepacket centred around $x = 3500$, a daughter wavepacket to the left of this, together with daughter and grandaughter wavepackets that are located successively to the right. The daughter wavepacket component positioned furthest to the left has propagated there along the leftward direction, while all three of the other components are rightward propagating.

Small amplitude disturbances that were detectable in experiments might be expected to display an even more complicated form of spatial variation, because the behaviour found at any given point in time would involve superpositions from wavepacket components arising from all possible sources of external forcing, and not just those that would have arisen, relatively cleanly, from a single impulsive and initially highly localised form of excitation. Thus if the spatio-temporal structure of the impulse response that we have considered here has the appearance of a family tree, but with possible overlapping between branches, then a corresponding space-time plot of the disturbance behaviour that would be expected for wavepackets in an actual physical experiment might bear more than a passing resemblance to a distant tangled *forest* of trees, growing upwards on a

sloped terrain. The slope would need to be incorporated into the picture in order to account for the fact that the roots of the trees would be found at different heights, corresponding to the different points in time at which they were triggered. Wherever the branches of either a particular tree, or different trees rooted at different heights, were found to cross and hence lie in the same line of sight, then there would be the possibility of a transient form of growth being found there.

3.4. *Consistency with simulation results obtained for monochromatic disturbances*

For further validation of our linearized simulation results, we recreated all of the features of the family-tree like disturbance structures that were shown in figures 1a and 2, by combining data obtained from a large set of separate numerical simulations, each conducted for a mononchromatic form of disturbance. For every distinct simulation, all of the perturbation flow variables were assumed to have a streamwise dependency $\sim \mathrm{e}^{iax}$, for a prescribed wavenumber a. As a consequence, the streamwise spatial derivatives which appear in the governing equations in §2 could simply be replaced with multiplication by ia. (More details about the implementation of such an approach can be found in Thomas *et al.* (2010).) The wavenumbers were sampled over a range of discrete values separated by a constant increment $\Delta a = 0.001$. The forcing needed to trigger the perturbations was applied using a wall-motion induced impulse, with exactly the same prescribed temporal variation as before, given by equation (2.5). The corresponding, highly localised, streamwise structure of the impulse was matched by specifying a set of wall-height amplitudes to weight the contribution made for each distinct wavenumber value. However, the impulse thus constructed necessarily has a spatial periodicity with a period $X_p = 2\pi/\Delta a \sim 6300$. This same artificial periodicity is inherited by all of the perturbation flow fields for the developing disturbance. For the evolution times that were to be considered, it was already known that non-periodic computational domains with a streamwise extent $X = 6000$ were sufficient to avoid spurious effects arising from the computational boundaries. Thus taking $X_p > 6000$ was expected to preclude the appearance of any non-physical spatial periodicity in the disturbance structure when the results from the monochromatic simulations were combined. This was confirmed to be the case.

3.5. *Wavenumber spectrum*

The wavenumber power spectra for the wall vorticity at selected times obtained from a simulation at $R = 725$ is shown in figure 4. (Similar results were obtained for the $R = 700$ simulation, except that the peak values displayed in the spectra decreased rather than increased with time.) Interestingly, the plots demonstrate that there is no selection of wavenumbers that would represent any periodicity on the larger length scales ~ 1000 units that characterise the branching structures for the family tree of wavepacket components. In view of this, some further checks were made to compare the results for the spatial-temporal development against those obtained by combining data from sets of monochromatic simulations. It was found that good agreement could still be retained in cases where the range of discretely sampled wavenumbers had a non-zero lower cut off that deliberately excluded the representation of wavelengths as large as the distances that developed between the different wavepacket components of the disturbance.

It may be seen that the wavenumber spectra, which are depicted for the times $\tau = \pi, 3\pi$ and 5π, show distributions that are centred within progressively narrow regions around values of a that are given approximately as 0.335, 0.355 and 0.365, respectively. The wavenumber at these peaks seems to be approaching the value of 0.375, the wavenumber predicted by Floquet analysis to have the largest temporal growth rate at the given Reynolds number (Blennerhassett & Bassom 2002). The corresponding wavelength is

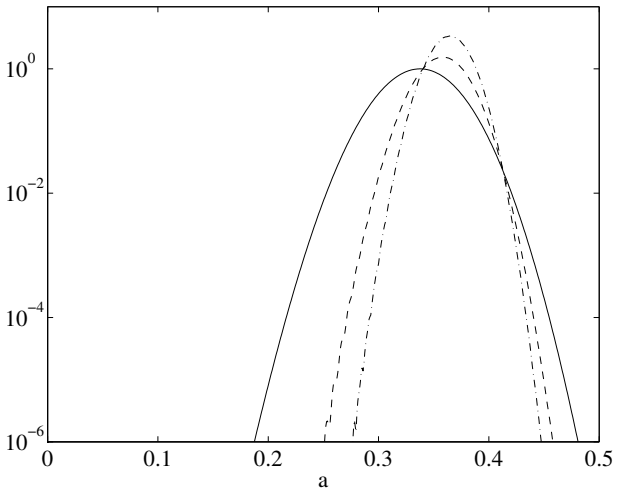

FIGURE 4. Wavenumber power spectra for the perturbation wall vorticity from a simulation with $R = 725$. Plots are shown for the times $\tau = \pi$ (solid), 3π (dashed) and 5π (chain). They were normalised by setting the peak value to unity for $\tau = \pi$.

$\lambda \sim 15$, so it may be seen immediately from figures 1a and 2 that the individual mother, daughter and grand-daughter wavepacket components of the disturbance are typically extended over a distance $\sim 10\lambda$. This spread is presumably determined by dispersion and diffusion effects, in the manner that is usual for perturbation wavepackets that evolve from a localised impulse. The spatial structure that distinguishes the separate branches of the family-tree for the disturbance development, which is defined over the relatively large length scale $\sim 50\lambda$, must therefore be attributed to the propagation of different wavepacket components. These are orientated to propagate along either the positive or the negative x-direction, depending on the phase of the basic flow oscillation at the time of their creation. It thus appears that the sizes of the most extended features of the disturbance are dictated by the distances travelled by smaller, more localised, perturbation components, which are themselves associated with wavenumbers that display an increasingly sharp distribution around a single value.

3.6. *Absolute instability and temporal growth*

The disturbance behaviour at any fixed point in space was typically found to exhibit a rather complicated time history, which could involve huge variations in magnitude over each oscillation cycle of the basic state. After a careful examination of the simulation data, we were unable to uncover any firm evidence of absolutely instability, at least for the values of the Reynolds numbers that it was feasible for us to consider. These values were restricted to being no more than only slightly above the threshold where Floquet modes of disturbance first become unstable. Thus it remains conceivable that a future theoretical analysis, conducted along the lines described by Brevdo & Bridges (1997), might demonstrate that the flow is in fact susceptible to absolute instability.

For the impulse response in steady flows, it is well known that over a long enough time interval, the maximum in the disturbance wavepacket amplitude will increase or

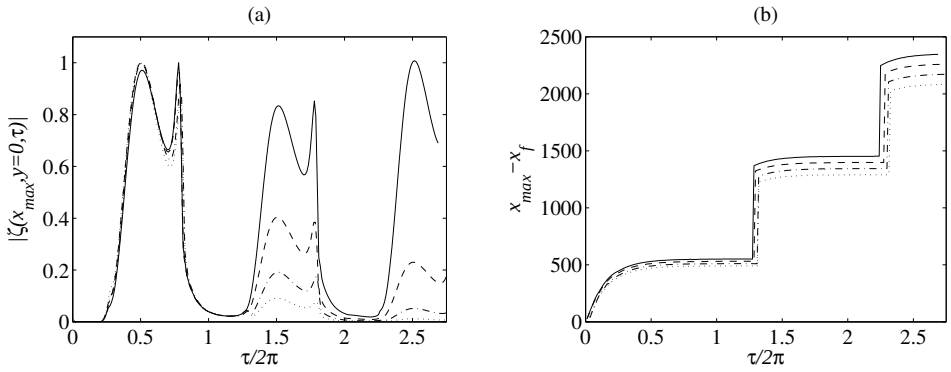

FIGURE 5. (a) Temporal development of the maximum amplitude of the perturbation vorticity at the wall for $R = 725$ (solid line), $R = 700$ (dashed), $R = 675$ (chain) and $R = 650$ (dotted); (b) Propagation of the maximum considered in (a), where x_{max} denotes the streamwise position at which the maximum occurs for any given instant of time

decrease at a rate that can be computed using the largest value for the temporal growth that is associated with a monochromatic form of disturbance with a prescribed spatial wavenumber. (A general account of this result can be found in Huerre & Rossi (1998) and an illustrative application is described in Davies (2003).) Thus we anticipated that, for the unsteady flow that is being considered here, some further connection between the predictions of Floquet theory and the behaviour found in the numerical simulations would be uncovered by considering the temporal development of the largest amplitudes displayed by the disturbance. This was found to be the case, as will be documented shortly in §3.8.

3.7. *Development of the disturbance maximum amplitude*

We first give a general illustration of the temporal development and spatial propagation of the maximum in the disturbance amplitude. It is again convenient to consider the perturbation vorticity magnitude $|\zeta|$ at the wall; figure 5a shows plots of the time histories of the maximum values. The data lines display the evolution that was determined from numerical simulations which were conducted at four equally spaced Reynolds numbers $R = 725$ (solid line), 700 (dashed), 675 (chain) and 650 (dotted). In each case, the disturbance amplitudes have been normalised using the greatest value that was attained over the course of the first period of oscillation, in order to ensure that all of the time histories could be plotted using a comparable vertical scale. It is interesting to note that, despite the fact that it is the impulse response that is being considered here, the development has very similar qualitative features to what was found by Thomas *et al.* (2010) for disturbances that had just a single prescribed wavenumber. Comparing magnitudes from the first to the second cycle, it may be observed that there appears to be a net decay for all four of the selected Reynolds numbers. This still occurs when $R = 725$, even though Blennerhassett & Bassom (2002) have demonstrated that the flow should then be linearly unstable. However, a further inspection of the disturbance development over the second and third cycles indicates that the magnitudes do in fact eventually begin to increase in the case where $R = 725$.

As has been illustrated earlier, an interesting feature of the disturbance development is the apparent regularity in the spacing for the streamwise locations of different wavepacket components. It was noted that the distances between the locations where the amplitudes of each mother, daughter and grand-daughter takes on their highest values were typically

almost two orders of magnitude larger than the wavelengths displayed within individual wavepackets. This means that the streamwise extent of the disturbance grows much more rapidly than would be possible if only a single wavepacket component was created from the initial impulse, as is commonly the case for disturbances triggered in a steady boundary layer flow. Figure 5b presents results that provide a systematic measure for the extent of the disturbance propagation away from the centre of the impulse that was used to trigger it. Letting x_{max} denote the location of the maximum amplitude of the perturbation wall vorticity, at any specified instant of time, the distance $x_{max} - x_f$ can then be used to quantify how far the disturbance has travelled. This distance is plotted against time over three cycles of oscillation, for the same set of Reynolds numbers that was considered in figure 5a. If we follow the path that was determined for $R = 650$ (dotted line), we see that, as the time progresses, the distance that has been travelled settles, initially, towards a value of approximately 500. It then jumps sharply at about the time $\tau = 2.6\pi$ and then again, at the same phase in the next oscillation cycle, near $\tau = 4.6\pi$, before it asymptotes to values of approximately 1300 and 2100, respectively. Very similar behaviour is found for all of the other Reynolds numbers. The sharp increases in the propagation distances correspond to when the location of the maximum amplitude has shifted, rightwards, from the mother wavepacket component to the daughter component and then, in turn, on to the grand-daughter component. The plots also indicate that the distances $x_{max} - x_f$ generally increase with the Reynolds number. For $R = 725$ this distance is approximately 2400 during the third cycle of the base flow oscillation, compared with 2100 for $R = 650$.

3.8. *Asymptotic temporal growth rates for the disturbance maximum*

Having given some indication of how the largest disturbance amplitudes develop and propagate, we now proceed to consider their temporal growth rate. This was measured by setting

$$\tilde{\mu}_r(\tau) = \ln\left(\frac{\max_{(x,y)}|\zeta(x,y,\tau+T)|}{\max_{(x,y)}|\zeta(x,y,\tau)|}\right)\Big/T, \tag{3.1}$$

where $T = 2\pi$ is the period for the base flow oscillation. For simplicity, the perturbation vorticity is again used to quantify the amplitudes, although it was convenient to no longer confine attention to the location of the wall. The maximum across the boundary layer has been deployed, rather than just the wall value. However, it is the determination of a maximum amplitude along the streamwise direction of the boundary layer that matters most here. The choice of some other physically appropriate local measure to specify the disturbance amplitude at each streamwise position would be expected to yield very similar growth rates.

Figure 6a depicts results for $\tilde{\mu}_r$ that were determined directly from the simulation data. The growth rate was calculated at intervals of $\Delta R = 25$ for the same time phase in the oscillation cycle, for each of the first three periods. The solid line displays the results obtained from the first cycle, the dashed the second and the chain the third (which is incomplete). The data for this third cycle is only partial due to the spreading of disturbances across the full streamwise extent of the computational domain, which meant we were unable to continue the numerical simulations for $R = 700$ and 725 very much beyond the range of times that are illustrated in figure 2a, namely, $\tau \lesssim 5.2\pi$. For the first two successive oscillation cycles, there are interceptions with the zero net growth rate axis at approximately $R = 730$, 718. A simple extrapolation of the data for the third cycle would suggest an intercept at around $R = 713$. It would thus appear that the variation with the Reynolds number of the computed growth rates is steadily

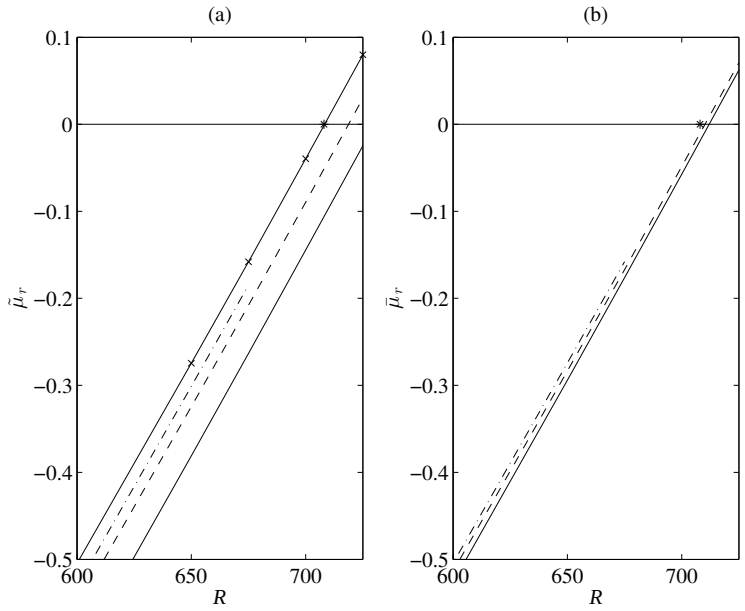

FIGURE 6. (a) Computed growth rates $\tilde{\mu}_r$, as defined by equation (3.1), plotted against R for the first (solid line), second (dashed) and third cycles (chain) of the base flow oscillation. The line which lies most to the left (with crosses and an asterisk at the axis intersection) was determined directly from Floquet theory. For each R, it shows the maximum value taken by the real part of the Floquet exponent μ_r, over the range of all spatially monochromatic waves; (b) as for (a) except that the growth rates are computed after accounting for an algebraic factor in the expected asymptotic development of the disturbance maximum. The line obtained from Floquet theory has been omitted, since it is indistinguishable from the amended growth rates for the third cycle.

approaching a form that exhibits good agreement with the prediction of neutral stability for $R_c \sim 708$ (indicated by an asterisk) derived from Floquet theory. Figure 6a also includes a line, passing through the marked neutral point, which represents the largest value that is taken by the real part of the Floquet exponent at each Reynolds number. It may be observed that, with each successive cycle, the values of the growth rate $\tilde{\mu}_r$ appear to be getting closer and closer to those that are given along this line.

The usual expression that can be derived to describe the long time asymptotic development of the maximum for wavepackets developing in steady boundary layers contains a diminishing factor of $1/\sqrt{\tau}$ that modifies the exponential growth or decay. Figure 6b displays growth rates $\bar{\mu}_r$ that have been amended to incorporate this additional factor. All of the plotted lines are labelled just as before. The collapse of the simulation data points on to the values predicted by Floquet theory is enhanced, with a more rapid convergence between successive cycles of the basic flow oscillation. In fact, by the third cycle, the computed growth rates cannot be visually distinguished from those determined from Floquet theory. This provides further confirmation that the long term development of the maximum amplitude of the impulsively excited disturbance is dictated by the largest temporal growth rate that can be obtained for monochromatic perturbations.

3.9. *Disturbance development across the boundary layer*

In the descriptions of the disturbance evolution that have been given up until now, we have focussed upon on the spatial structure along the x-direction aligned with the ba-

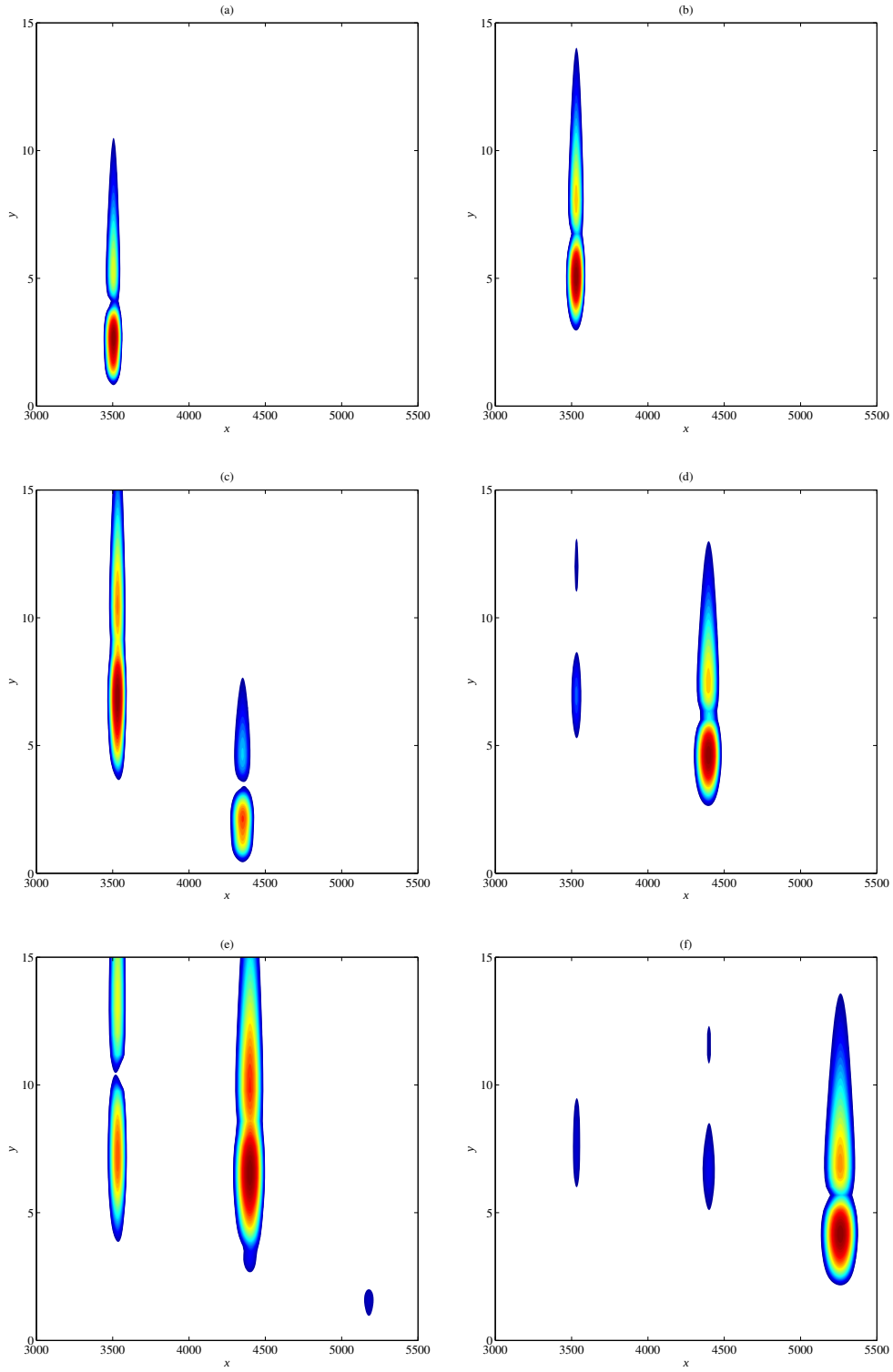

FIGURE 7. Snapshots of the streamwise velocity perturbation magnitude $|u|$ in the x-y plane for $R = 700$. The magnitudes are shaded using a logarithmic scaling, normalised using the maximum value attained at the chosen time instant. Subplots (a)–(f) are taken for the times $\tau/\pi = 0.9, 1.8, 2.7, 3.6, 4.5$ and 5.4, respectively, during the first three cycles of the base flow oscillation. (As was the case in the previously displayed magnitude plots for the wall vorticity, $|u|$ has been determined by applying a Hilbert transform to the simulation data, in order to construct envelopes for the x-dependent oscillatory variation of u.)

sic flow. We will now briefly illustrate the corresponding disturbance development that occurs across the boundary layer. Figure 7 displays the spatial variation within the x-y plane for the magnitude of the streamwise velocity perturbation u, at six equally separated time instants, taken over three cycles of the base flow oscillation. The Reynolds number is $R = 700$ and, as before, the disturbance was originally triggered at the streamwise location $x_f = 3000$. We focus on the behaviour that was found to the right of this location, which matches the orientation of the wall motion when the impulse was applied. The scale that is used for the shading is renormalised at each individual time instant, so that the positions where the amplitudes are largest can be more readily discerned. For the first two time instants considered, during the first oscillation cycle where $\tau = 0.9\pi$ and $\tau = 1.8\pi$, only the mother wavepacket component can be discerned, centred at around $x = 3500$. The largest perturbation values for this component are initially found close to the bounding wall, but as time passes they move steadily outwards across the boundary layer. In fact, it may be seen that this upwards trend continues throughout the whole of the period of time for which the six different plots are displayed. Moreover, it can be observed that as the mother component moves further away from the wall, the perturbation that it comprises has a diminishing magnitude, compared to what is found for other components of the disturbance, which arise at the later times. By the time that the third snapshot is taken, for $\tau = 2.7\pi$ in the second cycle of oscillation, a daughter wavepacket component has been born and subsequently moved near to $x = 4400$. This provides the dominant component of the disturbance at the next two times $\tau = 3.6\pi$ and $\tau = 4.5\pi$, before the largest amplitudes shift to the grand-daughter component, which is found in the vicinity of $x = 5700$ for the last of the plots at $\tau = 5.4\pi$. It may be noted that, just as for the mother component, the largest perturbation values for the daughter wavepacket component are initially displayed close to the wall, but they move outwards across the boundary layer as time passes, and diminish relative to the grand-daughter after this component has been born. Thus the simulation results presented in figure 7 illustrate a process where successive generations of perturbations are born, close to the wall, each from a parent whose individual fate is a fading away from prominence, which progresses in conjunction with a shifting motion that casts them outwards across the boundary layer.

3.10. *Phase dependence of the impulse response*

For the simulations that have been reported thus far, the disturbances have always been excited at the phase of the basic state oscillation that coincides with setting the time as $\tau_e = 0$ in equation (2.1). It will now be shown that if there is a change in the phase at which the impulse is applied, then although most of the quantitative details of the disturbance evolution are changed, the broader qualitative features remain very much the same. Figure 8 displays the development of four distinct perturbation structures, each for a disturbance excited at $R = 650$. The phase where the impulse is imposed has been varied across the discrete set of times $\tau_e = 0, \pi/4, \pi/2$ and π, respectively. (Note that, for ease of comparison, the time axis in all four of the plots has been labelled so that the impulse is located at time zero.) It may be seen that the main features of the disturbance evolution are similar in all of the four cases considered, with the development of a mother wavepacket component and subsequent daughter and grand-daughter wavepacket components. When the impulsive forcing is commenced at the three times with $0 \leqslant \tau_e \leqslant \pi/2$, in the first quarter of the oscillation cycle, the wavepacket components which have the largest magnitude propagate to the right, just as was observed for all of the simulations that were reported earlier. However, the distances over which the disturbances travel and spread, away from the impulse location, are generally decreased as τ_e is increased.

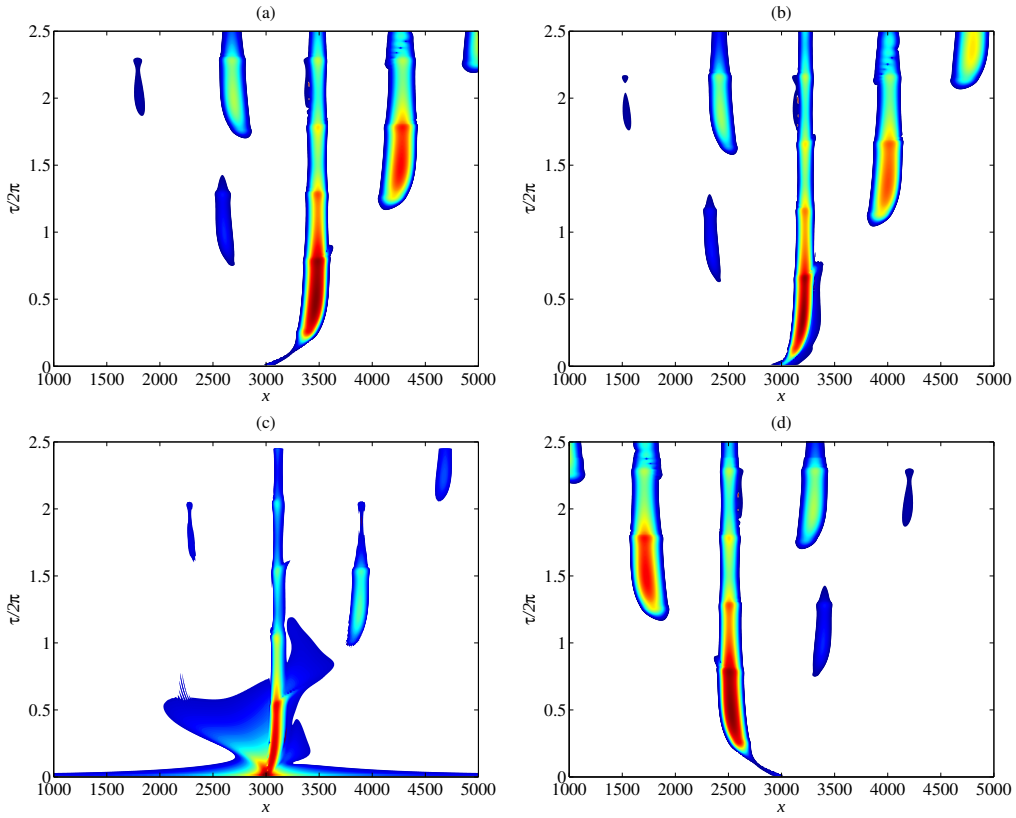

FIGURE 8. Spatial-temporal development of perturbation vorticity $|\zeta|$ at the wall, for $R = 650$. The disturbances were impulsively excited at $x_f = 3000$ and (a) $\tau_e = 0$; (b) $\tau_e = \pi/4$; (c) $\tau_e = \pi/2$; (d) $\tau_e = \pi$.

The last plot shown in the figure is for the case $\tau_e = \pi$, where the disturbance develops within a base flow for which the velocities are exactly reversed from those for $\tau_e = 0$; it may easily be seen from (2.1) that $U_B(y, \tau + \pi) = -U_B(y, \tau)$, for all times τ and vertical heights y. As should be expected, the spatial-temporal structures for $\tau_e = 0$ and $\tau_e = \pi$ are related to each other by a precise reflectional symmetry about a vertical line drawn through the forcing location $x_f = 3000$. After the half-period shift in the phase of the impulse timing, the larger magnitude perturbation components now propagate to the left, rather than to the right, but apart from this change in orientation the behaviour is identical. (It should be remarked that the mirror imagery, observed between plots 8a and 8d, provides confirmation that the previously discussed artificial asymmetry, which was imposed in the treatment of the streamwise limits of the computational domain, has not in any significant way affected the disturbance development.)

4. Nonlinear disturbance development

The effects of nonlinearity on the development of disturbances in the Stokes layer were studied by re-introducing the previously neglected nonlinear terms into the transport equation (2.3a) for the perturbation vorticity. We will illustrate how the novel structure

of the linearised disturbances may be built upon, with nonlinear mechanisms leading to significant changes in the vorticity distribution within wavepacket components.

4.1. *Some computational issues*

As was noted earlier, when the numerical methods were discussed, successful simulations for the nonlinear disturbance evolution required significant reductions in the streamwise grid size and the time step that were deployed in the discretization. Though these refinements greatly increased the computational expense that was incurred, they were necessary for capturing shorter scale structural features that arose from nonlinear interactions. By contrast, the spectral accuracy obtained from the use of a Chebyshev discretization for the wall-normal variation meant that there was no need to utilise any greater number of Chebyshev polynomials than had proved adequate for the linearized simulations.

To mitigate the costs of increasing the streamwise resolution, the streamwise length of the computational grid had to be reduced from $X = 6000$ to $X = 2000$. It was then imperative to ensure that nonlinear effects on the development were established relatively quickly, well before disturbances propagated over the shortened distances to the computational boundaries. This required a careful selection of the initial size for the impulsively excited disturbance, which was controlled by the value of the amplitude A that appears as a multiplier in the expression for the forcing given by equation (2.5). When the amplitude was taken to be relatively large, $A \sim 10^{-2}$, the development of nonlinear structures could be triggered almost instantaneously, within a small fraction of the base flow oscillation period. However, if the initial forcing was chosen to be too small, say with $A \sim 10^{-8}$, then any effects due to nonlinearity would not have appeared until the second or third cycle of the oscillation, resulting in excessively long execution times for the simulations. This would have been exacerbated by the need to reinstate the computational domain to have the same large streamwise extent that had been required for the studies of linearized disturbances.

4.2. *Selection of the physical configuration for the simulations*

The consequence of taking all of the above considerations into account was that we chose to examine configurations where nonlinear effects first arose for the mother wavepacket component of the disturbance and became apparent during the first half period of the base flow oscillation cycle. A limitation of this choice is that we are unable to examine nonlinear interactions between different components in the family tree-like structure of the disturbance. A full investigation awaits a future study, which will require the use of improved methods and computational resources.

We will focus here on results which were obtained from one particular nonlinear simulation that was conducted for $R = 500$. This Reynolds number is considerably less than that at which the flow first becomes susceptible to any Floquet form of linear instability. Nevertheless, there is still sufficient transient growth in the disturbance for nonlinear effects to be manifest within the first half period of the base flow oscillation. The possibility of such a rapid onset of nonlinearity is not in fact in any way inconsistent with the results obtained from Floquet theory. When disturbances in the Stokes layer are decomposed into Floquet modes that have a temporal structure of the general form $f(t)\exp(\mu t)$, it is found that there can be huge variations over the oscillation cycle in the magnitude of the time-periodic function $f(t)$, provided the Reynolds number is taken to be large enough. (An illustration of this behaviour can be found in Thomas *et al.* (2010).) These changes in the magnitude of $f(t)$ can suffice to trigger nonlinear effects, even when the real part of the Floquet exponent μ is negative and thus predicts that there should be stability.

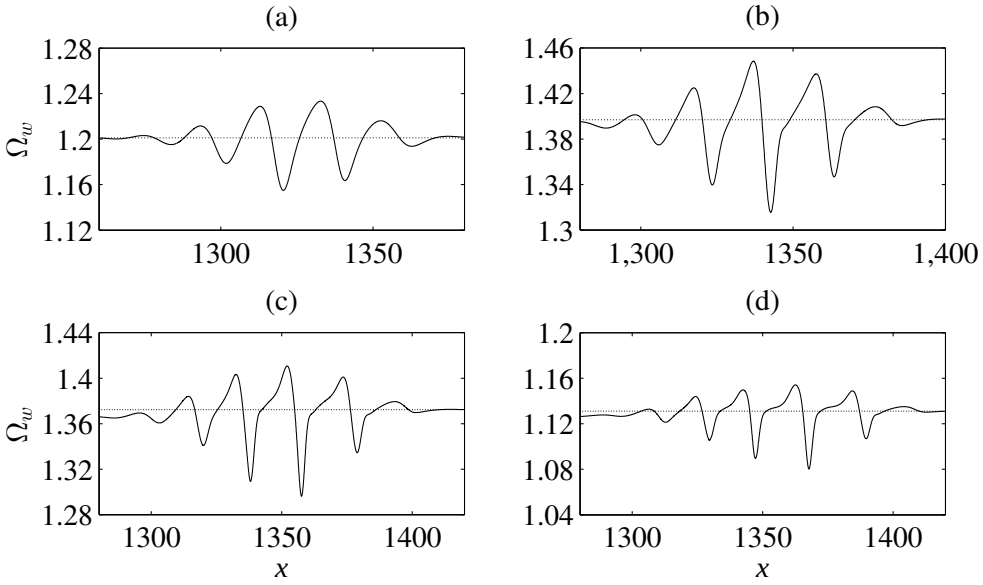

FIGURE 9. Total vorticity at the wall $\Omega(x, 0, \tau)$ for Reynolds number $R = 500$ and the times: (a) $\tau = 1.8$; (b) 2.2; (c) 2.6; and (d) 3. The impulse was centred at $x_f = 1000$ and applied for the time phase in the base flow oscillation given by setting $\tau = 0$ in equation (2.1). The dotted horizontal lines indicate the corresponding values of the base flow vorticity $U_B'(0, \tau) = \sin\tau - \cos\tau$.

The magnitude of the impulsive forcing was fixed by setting $A = 10^{-4}$, which created a disturbance that began by being small enough for its initial development to be essentially linear, but then grew sufficiently quickly for nonlinear effects to take hold within an acceptable frame of simulation times.

The qualitative form of the behaviour that will be reported may be taken as representative of what was discovered in similarly configured simulations, which were conducted for a selection of other relatively high values of the Reynolds number in the range $200 \leqslant R \leqslant 700$. In every case, structural features of the same general kind as those that we shall now describe were found to emerge during the nonlinear stages of the disturbance evolution. The most significant change to be found when the Reynolds number was increased was that the progression to nonlinearity became more rapid.

4.3. *Development of short scale features and the growth of spatial harmonics*

Figure 9 illustrates the time evolution of the total vorticity, $\Omega = \Omega_B + \zeta$, at the wall for four successive time instants. These were all taken within the second quarter of the first oscillation period after the initialisation of the disturbance by the impulsive forcing. In each case, the spatial variation is shown over a range of streamwise locations where the disturbance magnitudes are largest for the given point in time. From an inspection of the co-ordinate values marked on the x-axis, it may be seen that the disturbance is propagating in the direction in which x increases, which is opposite to the direction of the wall motion at all of the selected times. The time-varying value of the wall vorticity for the base flow is indicated in the plots by a dotted horizontal line. It may be observed that the magnitude of the perturbation vorticity has risen to become a fraction $|\zeta/\Omega_B| \sim 0.05$ of that for the base flow.

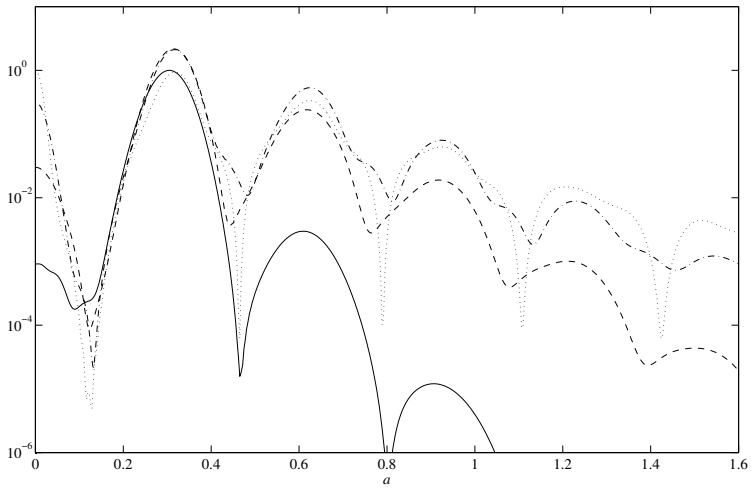

FIGURE 10. Wavenumber power spectra for the perturbation vorticity at the wall $\zeta(x, 0, \tau)$, from the nonlinear simulation conducted at $R = 500$. Plots are shown for the times $\tau = 1.8$ (solid line), 2.2 (dashed), 2.6 (chain) and 3 (dotted). To faciltate simplicity of comparison, the spectra have been artificially shifted so that the highest peak for the first chosen time instant takes a unit value.

The first of the snapshots of the total vorticity that are included in figure 9, which is for the time $\tau = 1.8$, displays a structure that involves a predominantly sinusoidal wave variation, together with a relatively simple modulation where the oscillation amplitude decreases in a monotonic fashion either side of the wavepacket maximum. It may readily be confirmed, from an inspection of the associated spectrum plotted in figure 10, that the disturbance can be characterized by a single wavenumber at this time instant. There is a very strongly dominant peak located at approximately $a_1 = 0.33$, which is in close correspondence with the value for the least stable wavenumber that would be expected from Floquet theory. An examination of the later development of the wall vorticity, which is displayed in figure 9 for the three subsequent time instants $\tau = 2.2, 2.6$ and 3, reveals that the disturbance evolves to become less and less sinusoidal and more and more 'spiky' in appearance. The manifestation of these sharpened features is a clear sign that nonlinear interactions have grown to play a significant role, inducing the development of smaller-scale structures in the disturbance. This behaviour can also be traced in the switching on of harmonics in the wavenumber spectra. The three remaining spectral data lines plotted in figure 10 were determined for the same time instants that we have just considered. They illustrate the generation of spectral peaks at integer multiples of the fundamental wavenumber $a = a_1$. As the time increases, it is possible to clearly pick out the growth of the harmonics located at $a_2 = 2a_1$, $a_3 = 3a_1$, as well as the modification of the mean flow represented by $a_0 = 0$. In fact, the utilization of the logarithmic scaling for the vertical axis makes it possible to discern the development of localised peaks for further higher order harmonics, though these are represented with a much reduced size.

4.4. *Wall pressure minima and vortical structures*

Plots that illustrate the development of the perturbation wall pressure are included in figure 11. It may again be seen that, after starting from an initially simple sinusoidal wave pattern, the disturbance evolves to display a more complicated streamwise variation.

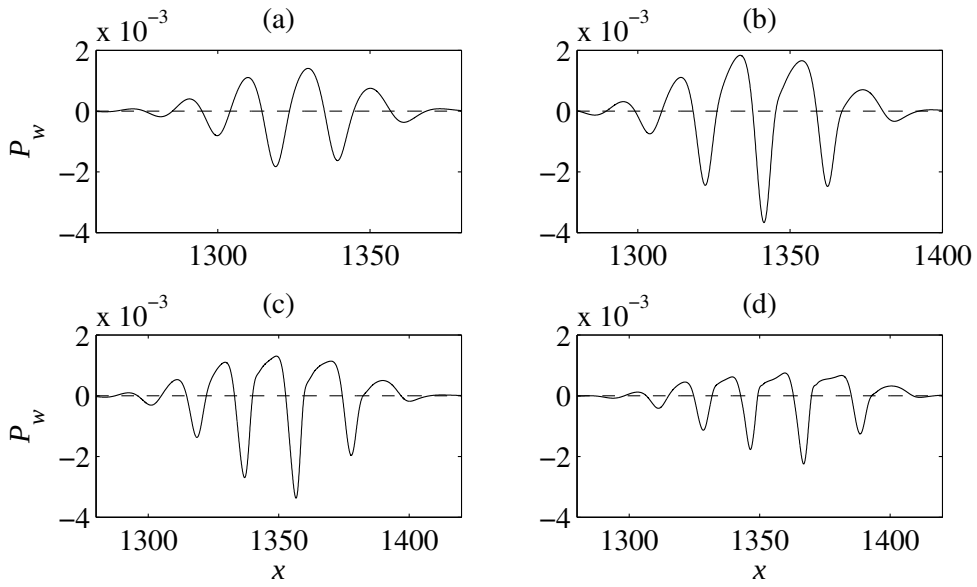

FIGURE 11. Perturbation pressure at the wall $p(x, 0, \tau)$, for $R = 500$ and the same time instants $\tau = 1.8$, 2.2, 2.6 and 3 that were considered in the two previous figures.

The behaviour of the pressure is characterized by the appearance of relatively sharp, but deep, negatively-valued minima. These are separated from each other by regions where the variation is more diffusely spread, with local maxima that are much less marked than the minima.

Figure 12 displays a visualization of a vortical structure that is typical of what it is found for the development of the nonlinear disturbance at later times. The spatial variation of the total vorticity is plotted across a region of the (x, y) plane, using a shading for the contour levels that picks out features that are associated with a limited range of values centred around zero. The plot is for the same time instant that was considered in figure 11(d), but the behaviour has been depicted using a more restricted frame of streamwise positions. This frame was chosen so as to coincide with one of the locations where the wall pressure exhibits a minimum. Solid lines are drawn to show the zero contours that mark the separate edges of a sandwiched region of negative vorticity. It may be observed that there are two distinct patches of oppositely signed vorticity. These appear to have been formed together, as the consequence of a relatively small region of positive vorticity having become displaced upwards, away from the bounding wall. Note that in the absence of any disturbance, the zero contours for the total vorticity at this time would have simply been the horizontal straight lines $y \approx 2.2$ and $y \approx 5.4$.

4.5. *Similarities to nonlinear behaviour in a steady boundary layer*

Some of the behaviour that we have discovered for the nonlinear disturbance development within the Stokes layer is very strongly reminiscent of what was found in previously reported simulations for a rather different physical configuration, involving a steady rather than an unsteady base flow. Bowles, Davies & Smith (2003) have investigated the nonlinear evolution of two-dimensional Tollmien-Schlichting waves in the Blasius boundary layer. In figure 2(c) from this earlier study, there are plots of the streamwise variation of the wall vorticity and perturbation pressure that have a remarkably similar form to those that have been presented here. The generation of spike-like structures in the vorticity, as

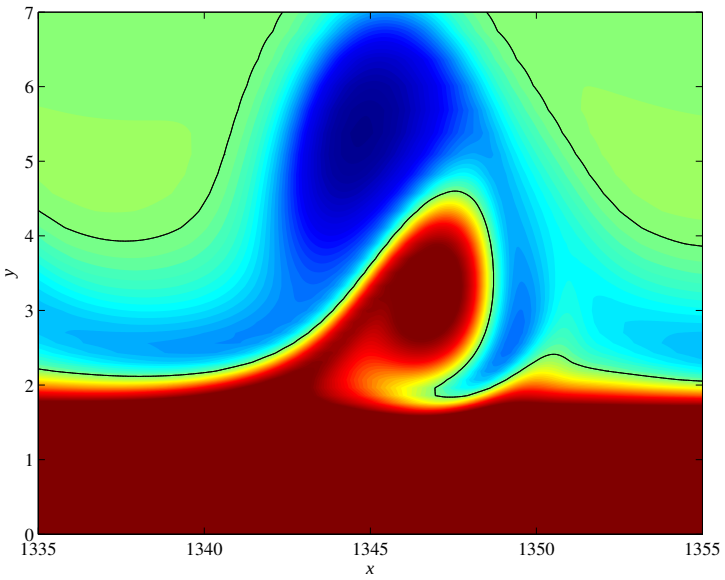

FIGURE 12. Total vorticity $\Omega(x, y, \tau)$ plotted in the (x, y)-plane for $R = 500$ at the time $\tau = 3$. The shading is chosen so as to highlight the appearance of structures in the range $-0.08 \leqslant \Omega \leqslant 0.08$. Solid lines are drawn for the two zero contours that enclose a region of negative vorticity. The wall vorticity associated with the basic state has the value $U_B'(0, \tau) = 1.13$ at this time instant.

well as sharp and deep pressure minima that are located between less pronounced pressure maxima, would appear to be features of the disturbance evolution that are common to both the Blasius and the Stokes layer flow. This degree of commonality suggests that some parts of the theoretical description that were given by Bowles *et al.* (2003), which relied upon results obtained from high Reynolds number asymptotic analysis, may also be applicable to the nonlinear disturbance behaviour that we have found in the unsteady setting of the Stokes layer. Any further elaboration and testing out of this rather speculative suggestion is left for future studies, as is the assessment of the significance of three-dimensional effects for the nonlinear disturbance development.

5. Closing remarks

We have conducted numerical simulations to study the development of disturbances in an oscillatory Stokes layer, triggered by a spatially localised impulse. The behaviour displayed for linearized perturbations turns out to be far more complex and interesting than has typically been found for steady flows. Rather than a single wavepacket, a novel family tree-like structure is determined, which is characterised by the birth of successive generations of distinct wavepacket components. We have shown that, despite the highly complex nature of the response, results obtained from a Floquet linear stability analysis can be used to describe various important features of the disturbance evolution. In particular, the dominant streamwise wavenumber and the temporal growth rate of the disturbance maximum can both be predicted in the limit of large times and a Fourier superposition in wavenumber space of linear eigenmodes leads to precisely the displayed

family-tree impulse response uncovered in the simulations. What is fascinating is that the now well established theory for the monochromatic eigenmodes (Blennerhassett & Bassom 2006) gave no hint of the complex flow structure that would follow from their physically appropriate combination.

The complicated spatial-temporal structure that is exhibited for the evolution of linearized disturbances suggests that it will be a challenging task to interpret any corresponding data that might be obtained from physical experiments. Moreover, the results discovered from the simulations that were conducted to study nonlinear behaviour make it plain that it is necessary to carry out physical experiments extremely carefully so that there is a very low level of external noise. Otherwise, nonlinear effects are likely to be manifested so quickly and strongly that it would be impractical to attempt to disentangle a stage in the development of disturbances that could be well described using linear stability theory. Our calculations indicated that at relatively early times after an impulse had been applied, growth associated with the establishment of the Floquet modal solution could be sufficient to generate a disturbance that was subject to significant nonlinear effects. Marked changes in the total vorticity distribution were seen to develop, even at Reynolds numbers well below the linear critical value, when the corresponding linearized disturbances would have been expected to suffer an eventual temporal decay. This behaviour is again likely to lead to problems in the interpretation of physical experimental results.

We thank the referees for many helpful comments regarding the interpretation and presentation of our numerical results.

This work was supported by the Australian Research Council grant DP0880463.

REFERENCES

Akhavan, R., Kamm, R. D. & Shapiro, A. H. 1991a An investigation of transition to turbulence in bounded oscillatory Stokes flows. Part 1. Experiments. *J. Fluid Mech.* **225**, 395–422.

Akhavan, R., Kamm, R. D. & Shapiro, A. H. 1991b An investigation of transition to turbulence in bounded oscillatory Stokes flows. Part 2. Numerical simulations. *J. Fluid Mech.* **225**, 423–444.

Blennerhassett, P. J. & Bassom, A. P. 2002 The linear stability of flat Stokes layers. *J. Fluid Mech.* **464**, 393–410.

Blennerhassett, P. J. & Bassom, A. P. 2006 The linear stability of high-frequency oscillatory flow in a channel. *J. Fluid Mech.* **556**, 1–25.

Blennerhassett, P. J. & Bassom, A. P. 2007 The linear stability of high-frequency flow in a torsionally oscillating cylinder. *J. Fluid Mech* **576**, 491–505.

Blondeaux, P. & Vittori, G. 1994 Wall imperfections as a triggering mechanism for Stokes-layer transition. *J. Fluid Mech.* **67**, 107–135.

Bowles, R. I., Davies, C. & Smith, F. T. 2003 On the spiking stages in deep transition and unsteady separation. *J. Eng. Math.* **45**, 227–245.

Brevdo, L. & Bridges, T. J. 1997 Absolute and convective instabilities of temporally oscillating flows. *Zeitschrift fr Angewandte Mathematik und Physik* **48**, 290–309.

Clamen, M. & Minton, P. 1977 An experimental investigation of flow in an oscillatory pipe. *J. Fluid Mech.* **77**, 421–431.

Clarion, C. & Pelissier, P. 1975 A theoretical and experimental study of the velocity distribution and transition to turbulence in free oscillatory flow. *J. Fluid Mech.* **70**, 59–79.

Cowley, S. J. 1987 High frequency Rayleigh instability analysis of Stokes layers. In *Stability of Time-dependent and Spatially Varying Flows* (ed. D. L. Dwoyer & M. Y. Hussaini), pp. 261–275. Springer.

Davies, C. 2003 Convective and absolute instabilities of flow over compliant walls. *Fluid Mechanics and its Applications* **72**, 69–93.

Davies, C. & Carpenter, P. 2003 Global behaviour corresponding to the absolute instability of the rotating-disc boundary layer. *J. Fluid Mech.* **486**, 287–329.

Davies, C. & Carpenter, P. W. 2001 A novel velocity-vorticity formulation of the Navier-Stokes equations with applications to boundary layer disturbance evolution. *J. Comp. Phys.* **172**, 119–165.

Davis, S. H. 1976 The stability of time-periodic flows. *Annu. Rev. Fluid Mech.* **8**, 57–74.

Eckmann, D. M. & Grotberg, J. B. 1991 Experiments on transition to turbulence in oscillatory pipe flow. *J. Fluid Mech.* **222**, 329–350.

Hall, P. 1978 The linear stability of flat Stokes layers. *Proc. R. Soc. Lond. A* **359**, 151–166.

Hall, P. 2003 On the stability of the Stokes layers at high Reynolds numbers. *J. Fluid. Mech.* **482**, 1–15.

Hino, M., Sawamoto, M. & Takasu, S. 1976 Experiments on transition to turbulence in an oscillatory pipe flow. *J. Fluid Mech.* **75**, 193–207.

Huerre, P. & Rossi, M. 1998 Hydrodynamic instabilities in open flows. In *Hydrodynamics and Nonlinear Instabilities* (ed. C. Godreche & P. Manneville), pp. 81– 294. Cambridge University Press.

von Kerczek, C. & Davis, S. H. 1974 Linear stability theory of oscillatory Stokes layers. *J. Fluid Mech.* **62**, 753–773.

Kloker, M., Konzelmann, U. & Fasel, H. 1993 Outflow boundary conditions for spatial navier-stokes simulations of transition boundary layers. *AIAA J.* **31**, 602–628.

Luo, J. & Wu, X. 2010 On linear instability of a finite stokes layer: instantaneous versus floquet modes. *Phys. Fluids* **22**, 054106.

Merkli, P. & Thomann, H. 1975 Transition to turbulence in oscillating pipe flow. *J. Fluid Mech.* **68**, 567–575.

Thomas, C., Bassom, A. P., Blennerhassett, P. J. & Davies, C. 2010 Direct numerical simulations of small disturbances in the classical Stokes layer. *J. Engng. Math.* **68**, 327–338.

Verzicco, R. & Vittori, G. 1996 Direct simulation of transition in Stokes boundary layers. *Phys. Fluids* **8**, 1341–1343.

Vittori, G. & Verzicco, R. 1998 Direct simulation of transition in an oscillatory boundary layer. *J. Fluid Mech.* **371**, 207–232.

Womersley, J. R. 1955 Method for the calculation of velocity, rate of flow and viscous drag in arteries when the pressure gradient is known. *J. Physiol.* **127**, 553–563.